© 2022. Published by The Company of Biologists Ltd | Journal of Cell Science (2022) 135, jcs258652. doi:10.1242/jcs.258652

RESEARCH ARTICLE

FMRP protects the lung from xenobiotic stress by facilitating the integrated stress response

Deblina Sain Basu[1,2], Rital Bhavsar[1], Imtiyaz Gulami[1,2], Saraswati Chavda[1], Sai Manoz Lingamallu[1,3], Ravi Muddashetty[1], Chandrakanth Veeranna[4], Sumantra Chattarji[1,5,6], Rajesh Thimmulappa[7], Aditi Bhattacharya[1,5] and Arjun Guha[1,*]

ABSTRACT

Stress response pathways protect the lung from the damaging effects of environmental toxicants. Here we investigate the role of the fragile X mental retardation protein (FMRP), a multifunctional protein implicated in stress responses, in the lung. We report that FMRP is expressed in murine and human lungs, in the airways and more broadly. Analysis of airway stress responses in mice and in a murine cell line *ex vivo*, using the well-established naphthalene injury model, reveals that FMRP-deficient cells exhibit increased expression of markers of oxidative and genotoxic stress and increased cell death. Further inquiry shows that FMRP-deficient cells fail to actuate the integrated stress response pathway (ISR) and upregulate the transcription factor ATF4. Knockdown of ATF4 expression phenocopies the loss of FMRP. We extend our analysis of the role of FMRP to human bronchial BEAS-2B cells, using a 9,10-phenanthrenequinone air pollutant model, to find that FMRP-deficient BEAS-2B cells also fail to actuate the ISR and exhibit greater susceptibility. Taken together, our data suggest that FMRP has a conserved role in protecting the airways by facilitating the ISR.

This article has an associated First Person interview with the first author of the paper.

KEY WORDS: Stress response, Lung, Integrated stress response, *FMR1*, FMRP

INTRODUCTION

The epithelial lining of the respiratory tract is continually challenged by a diverse array of environmental toxicants, including gases, particulates and biological agents. Exposure to these agents leads to increased oxidative, genotoxic and endoplasmic reticulum stress. Such stresses lead to cellular damage, inflammation and, in the long term, to lung damage and decreased lung functionality. The goal of this study was to probe the mechanisms by which lungs cope with environmental insults.

The capacity of the lung to manage xenobiotic stress is dependent on stress response proteins that are induced upon insult. In this regard, the integrated stress response (ISR) pathway is an evolutionarily conserved pathway that is integral to how the lung copes with environmental challenges (Pakos-Zebrucka et al., 2016; van 't Wout et al., 2014; Konsavage et al., 2012). The ISR is triggered by the activation of one or more of the four stress-responsive kinases GCN2 (also known as EIF2AK4), PKR (EIF2AK2), PERK (EIF2AK3) and HRI (EIF2AK1). The activation of these kinases, in turn, sets in motion two separate but interdependent processes that enable cells to mount a restorative response (Wong and Wispe, 1997). First, these kinases phosphorylate eukaryotic initiation factor 2α (eIF2α, also known as EIF2S1) and shut off ongoing programs of protein synthesis. The inhibition of translation leads to the sequestration of translationally active mRNAs into stress-induced condensates of various types. Second, activation of the kinases also induces specialized modes of protein translation, leading to the expression of stress response proteins. More specifically, these specialized translation regimes upregulate expression of activating transcription factor 4 (ATF4) (Pakos-Zebrucka et al., 2016; van 't Wout et al., 2014) and, in turn, ATF4 targets such as *ATF3*. ATF4 also synergizes with other transcription factors activated in response to stress, such as Nrf2 (NFE2L2), to induce the expression of stress response genes (He et al., 2001; Sarcinelli et al., 2020).

The fragile X mental retardation protein (FMRP, encoded by *FMR1*) is a multifunctional protein that is expressed in the brain and other organs, in humans and other animals alike. Deficiencies in FMRP lead to fragile X mental retardation syndrome (FXS), a disease characterized by mild-to-moderate intellectual disability (Zhou et al., 2014). FMRP function has been most intensively studied in the neuronal context, wherein the protein has been shown to regulate synaptic plasticity by multiple mechanisms (Santoro et al., 2012). Aside from this well-established role, several studies indicate that FMRP also has a role in facilitating stress responses. At a cellular level, FMRP has been shown to play an essential role in genesis of stress granules in response to arsenite and heat shock (Didiot et al., 2009; Linder et al., 2008). A recent study on fibroblasts derived from *Fmr1* knockout (KO) mice showed that FMRP is required for a specialized DNA damage response (DDR) in response to agents such as aphidicolin, 5-hydroxyurea (5-HU) and UV (Alpatov et al., 2014). The central finding of this study is that FMRP has a chromatin-dependent role in resolving stalled replication forks and single-strand breaks in DNA (Alpatov et al., 2014), but not in response to other types of genotoxic stress.

The lung is routinely exposed to a variety of environmental toxicants that cause many different types of stress. Our interest in mechanisms that regulate the pulmonary stress response led us to explore the role of FMRP in the lung. We immunostained murine and human lungs for FMRP to find that the protein is expressed in the airway epithelium and more broadly. To probe the role of FMRP in stress responses in the airways, we subjected *Fmr1* KO mice to

[1]Institute for Stem Cell Science and Regenerative Medicine (inStem), GKVK Campus, Bangalore 560065, India. [2]Trans Disciplinary University, Yelahanka, Bangalore 560064, India. [3]Manipal Academy of Higher Education, Madhav Nagar, Manipal 576104, India. [4]Department of Forensic Medicine, JSS Medical College, Mysore 570015, India. [5]Brain Development and Disease Mechanisms (BDDM), inStem, GKVK Campus, Bangalore 560065, India. [6]National Centre for Biological Sciences, GKVK Campus, Bangalore 560065, India. [7]JSS Medical College, JSS Academy of Higher Education & Research, Mysore 570015, India.

*Author for correspondence (arjung@instem.res.in)

R.B., 0000-0003-4646-2326; A.G., 0000-0002-3753-1484

Handling Editor: Kathleen Green
Received 17 March 2021; Accepted 8 March 2022

Journal of Cell Science (2022) 135, jcs258652. doi:10.1242/jcs.258652

naphthalene (Nap) injury, a well-established model for oxidative and genotoxic stress. We found that the airways of *Fmr1* KO mice exhibited higher expression of markers of oxidative and genotoxic stress, and greater cell death, than wild type. These findings led us to investigate the role of FMRP in airway stress responses, and in the ISR pathway, in mice and in the human lung.

RESULTS

FMRP is expressed in the airways and more broadly in the murine lung and protects airway club cells from Nap-induced stress

To characterize the role of FMRP in the pulmonary stress response, we examined the expression of the protein in adult lungs from wild-type (WT) and *Fmr1* KO animals. Lung sections from WT mice were stained with anti-FMRP antisera and examined under a confocal microscope (5 µm, *n*=8). FMRP expression was detected throughout the lung (Fig. 1A). We detected widespread protein expression in airway epithelium, both in secretory club cells (CCs, marked by expression of Scgb1a1, Fig. 1A,C) and in ciliated cells (marked by expression of acetylated tubulin, Ac-tub, Fig. 1A,C). Outside the airways, we noted intermittent expression in the alveolar parenchyma (Fig. 1A). Lung sections of *Fmr1* KO mice stained with the same anti-FMRP antisera did not show any specific staining (airways shown in Fig. 1B,D, *n*=3). Taken together, these experiments showed that FMRP is expressed in the murine lung, in the airways and more broadly. Next we examined hematoxylin and eosin (H&E)-stained lung sections from WT and *Fmr1* KO mice to compare morphologies of the lungs. We found that lungs from WT and *Fmr1* KO were comparable (Fig. S1A,B).

To investigate the role of FMRP in the pulmonary stress response, we focused our attention on FMRP-expressing airway CCs. Airway CCs are highly sensitive to the polycyclic hydrocarbon Nap (Stripp et al., 1995; Van Winkle et al., 1995). Nap administration leads to the loss of the vast majority of CCs from the airway epithelium within 24–48 h and is a well-established model for lung injury (Guha et al., 2014, 2017). The susceptibility of airway CCs to Nap is a result of the expression, in CCs, of the cytochrome P450 enzyme Cyp2f2 (Buckpitt et al., 2002). Cyp2f2 converts Nap to naphthalene oxide, which causes DNA damage. Naphthalene oxide is also converted to naphthoquinones, which cause oxidative stress (Buckpitt et al., 2002). Thus, to probe the role of FMRP in the pulmonary stress response in mice, we decided to utilize the Nap injury model. Interestingly, the Cyp2f2 isoform that converts Nap to cytotoxic derivatives is not expressed in humans and consequently Nap does not affect humans in the same way.

We exposed WT and *Fmr1* KO animals to Nap and harvested lungs for analysis at different timepoints post injury (regimen shown schematically in Fig. 1E). To assess the extent of injury, we quantified frequencies of CCs across timepoints and examined expression of markers of oxidative and genotoxic stress. We found that the frequencies of CCs in WT were significantly higher than in *Fmr1* KO at 12 h, 24 h and 48 h, respectively (Fig. 1F, *n*=3 mice per genotype per timepoint). In other words, cell loss was greater and faster in *Fmr1* KOs. Next, we stained sections from mouse lung prior to and post Nap injury with two antisera: anti-4-hydroxynonenal (4HNE, a product of lipid peroxidation and a marker of oxidative stress) and anti-γ-H2AX (a phosphorylated histone variant that is a marker of double-stranded DNA breaks and genotoxic stress). We did not detect expression of either marker in the lungs from uninjured WT and *Fmr1* KO mice (Fig. 1Gi,ii,Hi,ii). In contrast, the expression of both markers was dramatically increased in CCs in Nap-injured lungs (Fig. 1G,H). Pertinently, we noted that the levels of 4HNE and γ-H2AX expression in CCs were lower in WT than in *Fmr1* KOs at all timepoints examined (Fig. 1Giii–vi,Hiii–vi; see also the quantification in Fig. S1C,D, *n*=3 mice per genotype per timepoint). Based on these data, we concluded that CCs in *Fmr1* KO animals are more susceptible to Nap-induced stress.

The club-cell-like C22 cell line deficient in FMRP is also more susceptible to Nap-induced stress

To further probe the role of FMRP in stress responses in CCs, we turned to the murine club-cell-like cell line C22. C22 cells were derived from H-2Kb-tsA58 mice expressing a temperature-sensitive isoform of the SV40 large T antigen under the H-2Kb promoter (Demello et al., 2002). To characterize these cells, we stained C22 cells with markers of CCs and other airway and alveolar lineages. Consistent with previous reports, these cells expressed the CC marker Scgb1a1 (Fig. 2A) and did not express markers of other lineages (data not shown). We then performed a series of experiments to determine whether C22 could be utilized as a model for Nap injury, and to probe the role of FMRP therein.

First, C22 cells were stained with antisera against Cyp2f2 and FMRP. We found that C22 cells expressed modest levels of Cyp2f2 (Fig. 2B, *n*=6 experiments) and expressed FMRP (Fig. 2C, *n*=9 experiments). Next, we optimized methods for the knockdown of gene expression in C22 cells using siRNAs and methods for Nap challenge. We established that treatment with two different *Cyp2f2* siRNAs and three different FMRP siRNAs was sufficient to reduce Cyp2f2 and FMRP expression, respectively, by 80% or greater (see the Materials and Methods; compare Cyp2f2 or FMRP expression in scrambled siRNA-treated cells, Sc, and *Cyp2f2* or *Fmr1* siRNA-treated cells, Si, in Fig. S2A–C, *n*=3 experiments, and Fig. 2D, respectively, *n*=9 experiments). Careful titration of Nap dosage and time of exposure (see the Materials and Methods) showed that a 1 h pulse of Nap was sufficient to induce expression of oxidative and genotoxic stress markers in C22 cells and marginally increase cell death 24 h post exposure (see the Materials and Methods). We subsequently incubated control (scrambled siRNA-treated cells, Sc) and Cyp2f2-depleted (*Cyp2f2* siRNA-treated cells, Si) cells with Nap for 1 h and harvested cells at different timepoints for analysis (regimen shown schematically in Fig. S2D; see the Materials and Methods). Levels of 4HNE and γ-H2AX increased in Sc cells within 6 h and returned to baseline by 24 h (Fig. S2E–H, *n*=3 experiments each). In contrast, levels of expression in Si-cells remained at baseline levels at all timepoints (Fig. S2E–H, *n*=3 experiments each). These data showed that C22 cells are susceptible to Nap-induced stress in a Cyp2f2-dependent manner like CCs *in vivo*.

To explore the possibility that FMRP regulates susceptibility to Nap in C22 cells, we incubated control (scrambled siRNA-treated cells, Sc) and FMRP-depleted (*Fmr1* siRNA-treated cells, Si) cells with Nap for 1 h and then harvested cells at different timepoints for analysis (shown schematically in Fig. 2E). To assess levels of oxidative and genotoxic stress, we again stained cells with anti-4HNE and anti-γ-H2AX, respectively (Fig. 2F,H). In order to assess the cytotoxicity of Nap, we subject the cells to a WST-1 assay 24 h post exposure. We found that levels of 4HNE and γ-H2AX (Fig. 2F–I) were elevated in *Fmr1*-depleted cells at all timepoints (*n*=3 experiments each) and that *Fmr1*-depleted cells exhibited greater cell death in response to Nap (Fig. 2J). These data correlated well with the increased susceptibility of CCs to Nap in *Fmr1* KO animals and demonstrated that FMRP has a cell-intrinsic role in protecting cells from Nap.

Journal of Cell Science (2022) 135, jcs258652. doi:10.1242/jcs.258652

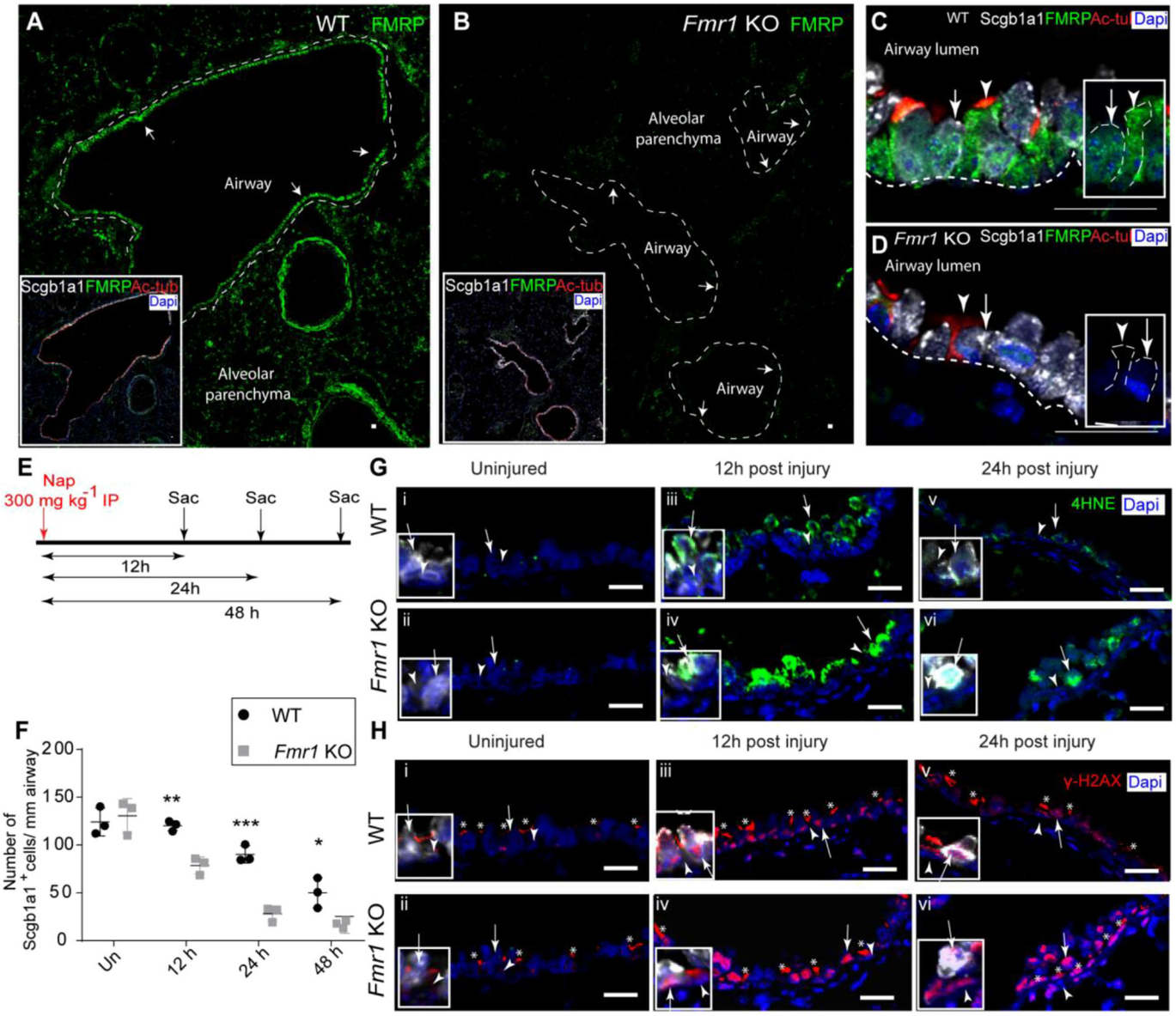

Fig. 1. FMRP is expressed in the airways and more broadly, and protects airway club cells from Nap-induced stress. (A–D) FMRP expression in the murine lung. (A) Tiled image showing FMRP immunostaining (green, white arrows) in the airway epithelium (demarcated by white dashed lines) and in the parenchyma of the murine lung. The airways are identified by expression of the club cell (CC) marker Scgb1a1 (white, inset) and of the ciliated cell marker acetylated tubulin (Ac-tub, red, inset). (B) Tiled image showing FMRP immunostaining in *Fmr1* knockout (*Fmr1* KO) mice. Note the absence of FMRP (green) in both airways (demarcated by white dashed lines, inset) and parenchyma. (C,D) High-resolution image of FMRP immunostaining (green) in airway epithelial cells. Here, CCs are shown in white (white arrow in inset) and ciliated cells are in red (white arrowhead in inset) in wild type (C) and *Fmr1* KO (D). (E–H) Susceptibility of CCs to Nap injury in control and *Fmr1* KO. (E) Schematic showing regimen for Nap injury. (F) Frequencies of Scgb1a1^{+} cells in wild type (black circles) and *Fmr1* KO (gray squares) from uninjured (Un) and Nap-injured mice at different timepoints post injury. Each data point in the scatter plot represents multiple sections from a single animal (n=3 mice) with mean±s.e.m. (G,H) Expression of markers of oxidative (4HNE) and genotoxic (γ-H2AX) stress in airways from wild-type and *Fmr1* KO mice prior to and post Nap injury. Note white arrowheads showing ciliated cells and white arrows showing CCs on the airways and in insets (counterstained with Scgb1a1 antisera, white). (G i–vi) 4HNE immunostaining (green) in the airways of wild-type (i,iii,v) and *Fmr1* KO (ii,iv,vi) mice prior to and post Nap injury. (H i–vi) γ-H2AX immunostaining (red) in the airways of control (i,iii,v) and *Fmr1* KO (ii,iv,vi) mice prior to and post Nap injury. Asterisks show cilia of ciliated cells marked with γ-H2AX (H i–vi). See also Fig. S1. Statistical significance was assessed by an unpaired two-tailed *t*-test: **P*<0.05; ***P*<0.01; ****P*<0.001. The changes in the two groups over time, across genotype and interaction parameters were also assessed by two-way ANOVA and found to be statistically significant. For Shapiro–Wilk normality test and two-way ANOVA, see Table S1. Scale bars: 20 µm.

FMRP is required for induction of the ISR pathway, which protects from Nap-induced stress

A role for FMRP in mediating stress responses has been reported previously. One of these studies has pointed towards a role for the protein in stress granule biogenesis in response to arsenite or heat shock (Didiot et al., 2009). This study suggests that FMRP may have a role in the induction of the ISR, a pathway necessary for stress granule biogenesis, or a more specific role in the induction of stress granule biogenesis, or both. As the ISR has been shown to be important for stress responses in the lung, we decided to examine the possibility that FMRP may be required for the induction of the ISR in C22 cells post Nap. We note that FMRP-deficient cells also fail to recruit γ-H2AX to stalled replication forks and single-strand breaks in response to aphidicolin, 5HU and UV

Journal of Cell Science (2022) 135, jcs258652. doi:10.1242/jcs.258652

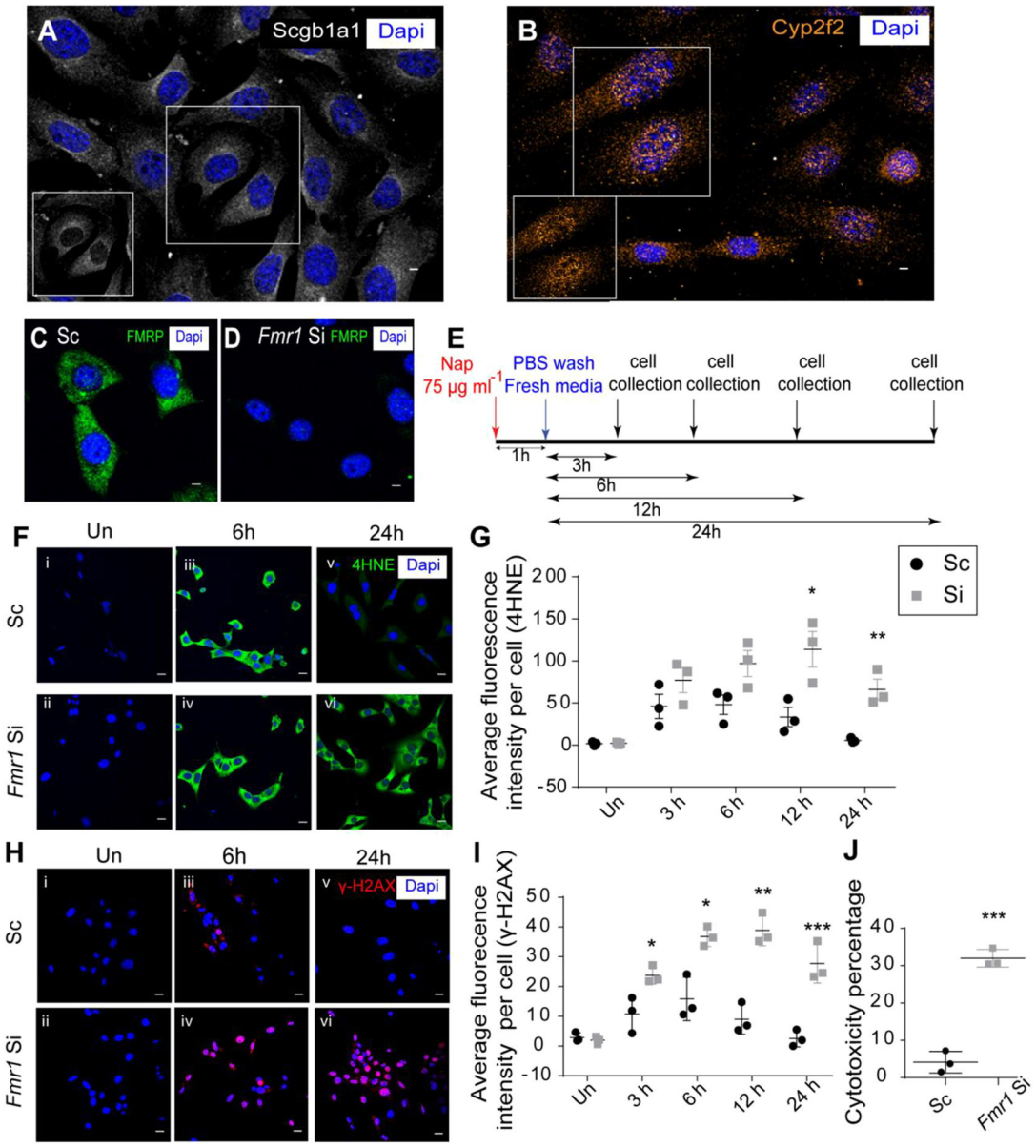

Fig. 2. FMRP-deficient club-cell-like C22 cells are susceptible to Nap-induced stress. (A–D) Phenotypic characterization of C22 cells. (A) Scgb1a1 immunostaining (white) in C22 cells. Inset shows Scgb1a1 staining alone in C22 cells from the same field. (B) Cyp2f2 (orange) immunostaining in C22 cells. Inset shows Cyp2f2 staining alone in C22 cells from the same field. See also Fig. S2. (C,D) FMRP immunostaining (green) in C22 cells treated with scrambled siRNA (C) and in C22 cells treated with *Fmr1* siRNA (D). (E–J) Susceptibility of C22 cells to Nap [control is scrambled siRNA-treated (Sc), and *Fmr1* siRNA-treated (Si)]. (E) Schematic showing regimen for Nap injury. (F–I) Expression of markers of oxidative (4HNE) and genotoxic (γ-H2AX) stress in Sc and Si cells prior to and post Nap. (Fi–vi) 4HNE immunostaining (green) in Sc and Si cells prior to and post Nap. (G) Quantification of 4HNE immunofluorescence per cell in Sc and Si cells prior to and post Nap. Un, uninjured. (Hi–vi) γ-H2AX immunostaining (red) in Sc and Si cells prior to and post Nap. (I) Quantification of γ-H2AX immunofluorescence per cell in Sc and Si cells post Nap. (J) Cytotoxicity of Nap in Sc and Si cells 24 h post Nap (*n*=3 experiments). For immunofluorescence analysis, ≥25 cells were analyzed per timepoint per experiment, *n*=3 experiments. Graphical data represent mean±s.e.m. Black circles, Sc; gray squares, Si. **P*<0.05; ***P*<0.01; ****P*<0.001 (unpaired two-tailed *t*-test). For normality test and two-way ANOVA, see Table S2. Scale bars: 5 µm.

(Alpatov et al., 2014). Although it is plausible that FMRP serves a similar role in Nap-treated cells, we noted that the nuclear accumulation of γ-H2AX in FMRP-deficient CCs and C22 cells post Nap was greater than in the respective controls. This suggested to us that the DDR was at least partially active in FMR-deficient cells and, more importantly, that extent of DNA damage (as reported by nuclear γ-H2AX accumulation) was greater in FMR-deficient cells than in controls (see the Discussion). Taken together, the findings led us to investigate the role of FMRP in the ISR pathway.

As previously mentioned, the ISR is induced when one of four stress-responsive kinases (GCN2, PERK, HRI, PKR) phosphorylate eIF2α at serine-51. Phosphorylation of eIF2α arrests conventional translation, promotes sequestration of mRNAs being actively translated and enables specialized translation of mRNAs encoding stress response proteins such as ATF4 (Pakos-Zebrucka et al., 2016; van 't Wout et al., 2014). To probe the status of the ISR in C22 cells post Nap, we examined the phosphorylation state of eIF2α. We exposed C22 cells to Nap for 1 h, harvested cells at various timepoints and quantified the levels of expression of both eIF2α and

Journal of Cell Science (2022) 135, jcs258652. doi:10.1242/jcs.258652

phosphorylated eIF2α (p-eIF2α). Western-blot-based ratiometric quantification of total and p-eIF2α in Sc cells showed that p-eIF2α levels increased 3 and 6 h post injury and decreased to baseline levels thereafter (Fig. 3A; Fig. S3A,B, *n*=5 experiments). We inferred that the ISR is induced in C22 cells in response to Nap. We then exposed Si cells to Nap for 1 h and found that, contrary to controls, the levels of p-eIF2α did not increase post Nap (Fig. 3A; Fig. S3A,B, *n*=5 experiments). The analysis of p-eIF2α suggested that FMRP depletion might inhibit the ISR.

Next, we examined the expression of ATF4 and its target, *ATF3*, in control and FMRP-deficient cells. Sc and Si cells were stained with an anti-ATF4 antibody prior to and post Nap treatment. In Sc, the expression of ATF4 was undetectable in untreated cells, increased dramatically at 3, 6 and 12 h post Nap treatment and then approached baseline levels at 24 h (Fig. 3B,C, *n*=5 experiments). In Si cells, levels of ATF4 were negligible in untreated cells and showed no appreciable increase post Nap treatment (Fig. 3B,C, *n*=5 experiments). Next, we assayed *ATF3* levels by quantitative real-time PCR (qPCR). For this, RNA was isolated from Sc and Si cells at different timepoints and subjected to qPCR analysis. In Sc, levels of *ATF3* mRNA increased at 3 and 6 h post Nap and returned to baseline thereafter (Fig. S3C, *n*=3 experiments). In Si, the *ATF3* levels did not rise appreciably above baseline post Nap (Fig. S3C). These findings were also validated with anti-ATF3 immunostaining (data not shown). Based on these data, we concluded that both ATF4 and ATF3 expression are perturbed in FMRP-deficient cells post Nap. Taken together, the findings showed that the ISR is perturbed in FMRP-deficient cells post Nap.

We also probed whether the upstream kinases that phosphorylate eIF2α and induce the ISR become activated (phosphorylated) in FMRP-deficient cells. We probed the expression of GCN2, PERK, HRI, PKR and their phosphorylated isoforms in Nap-treated C22 cells using commercially available antibodies (see the Materials and Methods). Among all pairs of antisera tested, antisera for PKR and p-PKR provided reproducible results. Western-blot-based ratiometric quantification of p-PKR and total PKR in Sc and Si cells showed that the p-PKR levels increase in both Sc and Si 3 h post Nap (Fig. S3D–F, *n*=3 experiments). Importantly, we noted that levels of p-PKR returned to baseline in Sc at 6 h and later timepoints, but remained significantly higher in Si at later timepoints (Fig. S3D–F). This suggested that at least one of the stress-responsive kinases (PKR) is activated in FMRP-deficient cells post Nap.

Perturbations to the ISR provided a plausible explanation for why FMRP-deficient C22 cells are more susceptible to Nap. To test this, we decided to probe how perturbing the ISR, by knocking down levels of *Atf4*, would impact susceptibility to Nap. Control (scrambled siRNA) and *Atf4* siRNA-treated C22 cells were exposed to Nap as described earlier and cells were harvested at different timepoints for

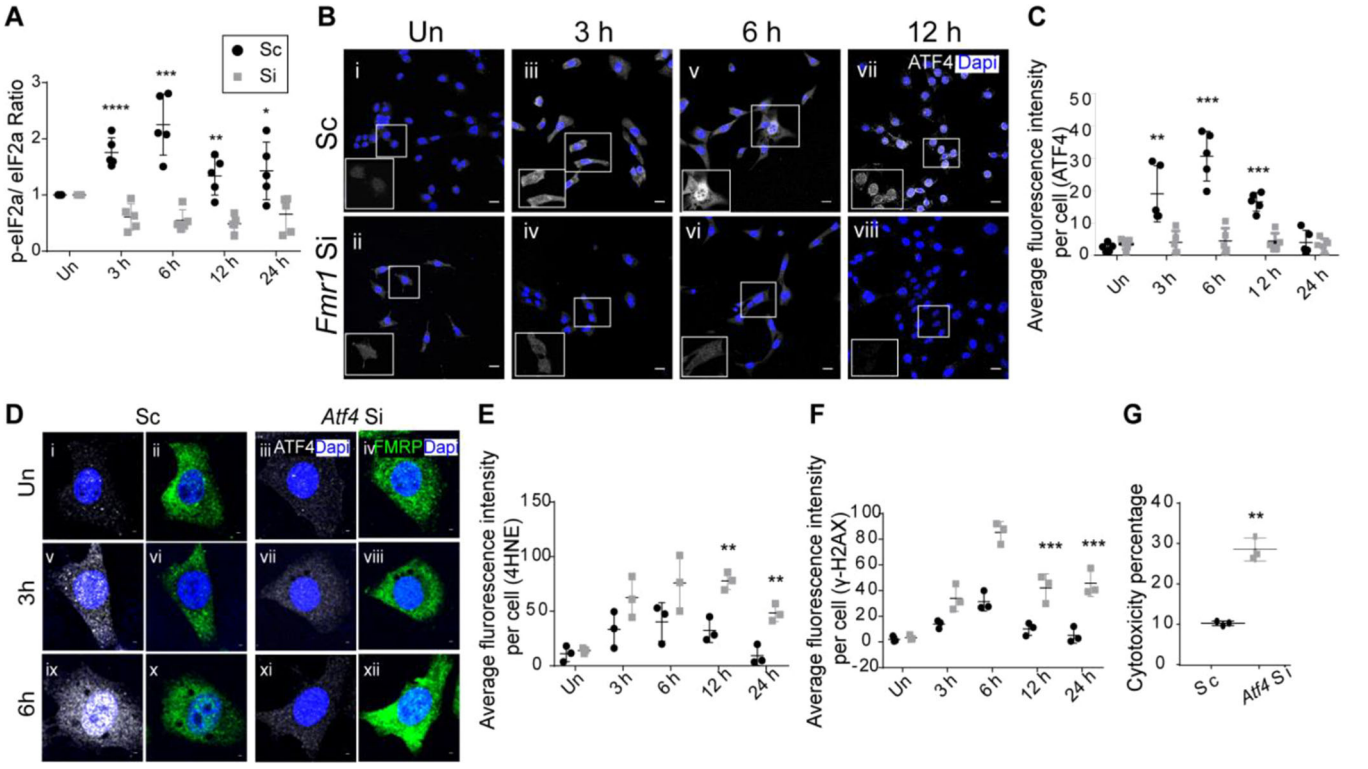

Fig. 3. FMRP-deficient C22 cells fail to upregulate the integrated stress response and to induce ATF4, essential for protection from Nap-induced stress. (A) Western blot-based quantification of phospho-eIF2α:eIF2α ratios in Sc and Si cells prior to and post Nap treatment (*n*=5 experiments). See Fig. S3 for representative blots used for quantification. Un, uninjured. (Bi–viii) ATF4 immunostaining (white) in Sc (i,iii,v,vii) and Si (ii,iv,vi,viii) cells prior to and post Nap. Note nuclear accumulation of ATF4 in Sc cells by 6 h post Nap (inset). (C) Quantification of ATF4 immunofluorescence per cell in Sc and Si cells prior to and post Nap (*n*=5 experiments). (D–G) Susceptibility of C22 cells to Nap in control (scrambled siRNA-treated, Sc) and *Atf4* siRNA-treated (Si) cells. (Di–xii) Analysis of ATF4 levels (white) and FMRP levels (green) in Sc and Si cells prior to and post Nap treatment. Immunostaining for ATF4 (white) and FMRP (green) in Sc (i,ii,v,vi,ix,x) and Si (iii,iv,vii,viii,xi,xii) cells. (E) Quantification of 4HNE immunofluorescence per cell in Sc and Si cells prior to and post Nap. See Fig. S3 for representative images. (F) Quantification of γ-H2AX immunofluorescence per cell in Sc and Si. See Fig. S3 for representative images. (G) Cytotoxicity of Nap in Sc and Si cells 24 h post Nap exposure (*n*=3 experiments). For immunofluorescence analysis, ≥25 cells were analyzed per timepoint per experiment. Graphical data represent mean±s.e.m. Black circles, Sc; gray squares, Si. **P*<0.05; ***P*<0.01; ****P*<0.001; *****P*<0.0001 (unpaired two-tailed *t*-test). For normality test and two-way ANOVA, see Table S3. Scale bars: 5 µm.

Journal of Cell Science (2022) 135, jcs258652. doi:10.1242/jcs.258652

analysis. ATF4 immunostaining of control and *Atf4* siRNA-treated cells showed that siRNA treatment eliminated ATF4 expression in cells post Nap exposure (Fig. 3D). We also found that ATF4-depleted cells exhibited increased expression of 4HNE (Fig. 3E; representative images shown in Fig. S3G) and γ-H2AX (Fig. 3F; representative images shown in Fig. S3H) at all timepoints examined (n=3 experiments each, quantification of cell fluorescence based on $n\geq25$ cells per experiment) and increased cell death 24 h post injury (Fig. 3G). We concluded that the increased levels of oxidative and genotoxic stress and increased cytotoxicity observed in FMRP-deficient cells could be the result of a failure to induce the ISR and upregulate ATF4.

In light of the findings in C22 cells, we examined whether perturbations to the ISR are also observed in FMRP-deficient CCs in Nap-treated mice. We counterstained sections from control and *Fmr1* KO lungs post Nap with antisera to both ATF4 and ATF3. Although ATF4 immunostaining was inconclusive, we noted that the levels of ATF3 were negligible in CCs in the control lung and upregulated post Nap (Fig. S3I,J, sections from n=3 mice). Pertinently, the levels of ATF3 in CCs in *Fmr1* KO did not increase post Nap. These results are consistent with a role for FMRP in the induction of ISR in CCs post Nap.

FMRP is expressed in the airways of the human lung and protects human bronchial BEAS-2B cells from 9,10-phenanthrenequinone-induced stress

The findings in the murine lung led us to ask whether FMRP has a conserved role in the human lung. To investigate this possibility, we first examined the distribution of FMRP in the human lung. Paraffin sections stained with FMRP antisera showed that FMRP is expressed throughout the airways and more broadly (Fig. 4Ai,ii,iv, n=2 sections each from n=5 independent lung biopsies). Triple labeling experiments with markers for ciliated cells and CCs showed that FMRP is expressed in both ciliated and non-ciliated cells, including CCs. Based on the distribution of FMRP, we surmised that the protein could also play a role in the airways in the human lung.

The BEAS-2B cell line is derived from normal human airways. These cells do not express markers of ciliated cells and, akin to CCs, have characteristics of non-ciliated cells. We stained BEAS-2B cells with FMRP antisera to find that these cells expressed FMRP (Fig. 4B, n=6 experiments). We then proceeded to develop an assay to probe the role of FMRP in stress responses in these cells.

Since the susceptibility of airway CCs to Nap is not recapitulated in the human lung or in BEAS-2B cells (data not shown), we utilized a different injury model to probe the role of FMRP in stress responses in human cells. 9,10-Phenanthrenequinone (PQ) is an air pollutant that is present at high levels in diesel exhaust particles and is known to trigger oxidative and genotoxic stress (Lavrich et al., 2018). As part of our characterization of PQ, we first exposed control (scrambled siRNA-treated cells) and FMRP-depleted (*Fmr1* siRNA-treated cells) C22 cells to a pulse of PQ for 1 h and harvested cells at different timepoints for analysis (data not shown). Consistent with our findings in the Nap model, we found that FMRP-depleted C22 cells exhibited increased expression of 4HNE and γ-H2AX and increased cell death 24 h post exposure (data not shown). We then examined ATF4 expression to find that although ATF4 levels increased in Sc cells at 3 h and 6 h post PQ, no expression was detected in Si cells (data not shown). These experiments showed that PQ treatment does lead to oxidative and genotoxic stress, and that FMRP-deficient C22 cells are more susceptible, and led us to examine the effects of PQ on BEAS-2B cells.

To test the role of FMRP in BEAS-2B cells, we determined that the protocol for the knockdown led to a 90% reduction in the levels of FMRP post treatment (Fig. 4B,C, n=6 experiments). Next, we exposed control (scrambled siRNA-treated cells) and FMRP-depleted (*FMR1* siRNA-treated cells) BEAS-2B cells to a pulse of PQ for 1 h and harvested them at different timepoints for analysis (shown schematically in Fig. 4D). We found that FMRP-depleted cells exhibited increased expression of 4HNE (Fig. 4E,F) and γ-H2AX (Fig. 4G,H) at all timepoints examined (n=3 experiments each, quantification of cell fluorescence based on $n\geq25$ cells per experiment) and increased cell death 24 h post injury (Fig. 4I). These experiments showed that FMRP-deficient BEAS2B cells are more susceptible to PQ.

FMRP is required for the induction of the ISR pathway, which protects from PQ-induced stress

Next, we determined whether FMRP is required for the induction of the ISR in BEAS-2B cells. As described previously, we probed the phosphorylation status of eIF2α (Fig. 5A; Fig. S4A,B, n=5), the levels of ATF4 induction (Fig. 5B,C, n=5) and the levels of *ATF3* induction (Fig. S4C, n=3), and the ratio of phosphorylation status of PKR (Fig. S4D–F) at different times post PQ. These experiments showed that although p-PKR levels were increased in both Sc and Si post PQ, all of the downstream processes of the ISR were perturbed in Si.

We then investigated whether the loss of ATF4 would recapitulate the loss of FMRP post PQ. Control (scrambled siRNA) and *ATF4* siRNA-treated BEAS-2B cells were exposed to PQ as described previously, and cells were harvested at different timepoints for analysis. Consistent with expectations, *ATF4* siRNA-treated cells showed no anti-ATF4 immunostaining post PQ exposure (Fig. 5D, n=3 experiments). We found that ATF4-depleted BEAS-2B cells exhibited increased expression of 4HNE (Fig. 5E; representative images shown in Fig. S4G) and γ-H2AX (Fig. 5F; representative images shown in Fig. S4H) and increased cell death 24 h post injury (see the Materials and Methods, Fig. 5G). These data indicated that the loss of ATF4 largely phenocopies the loss of FMRP in PQ-treated BEAS-2B cells.

The findings in BEAS-2B cells suggested that the role of FMRP in the actuation of the ISR pathway is conserved. To probe whether this finding is more broadly applicable to the lung, we performed the assays described above in another cell line of epithelial origin: A549 cells. We found that although A549 cells are of alveolar origin, they also express FMRP (Fig. S5A). Importantly, PQ exposure assays showed that A549 cells lacking FMRP exhibit higher levels of oxidative and genotoxic stress and fail to actuate ATF4 expression (Fig. S5B–I). Taken together, the studies in BEAS-2B and A549 strongly suggest that FMRP also regulates the induction of the ISR in the human respiratory epithelium.

DISCUSSION

The aim of this study was to probe the role of FMRP in stress responses in the lung. We report that FMRP plays an essential role in protecting the airways in mice, and potentially in humans, from the deleterious effects of xenobiotic stress. Our studies provide strong evidence that FMRP protects the lung by facilitating the induction of the ISR (see model, Fig. 6). In the paragraphs that follow we will discuss the plausible mechanism(s) by which FMRP may regulate the ISR, the possibility that FMRP regulates stress response pathways in addition to the ISR, and the clinical implications of the findings reported here.

Journal of Cell Science (2022) 135, jcs258652. doi:10.1242/jcs.258652

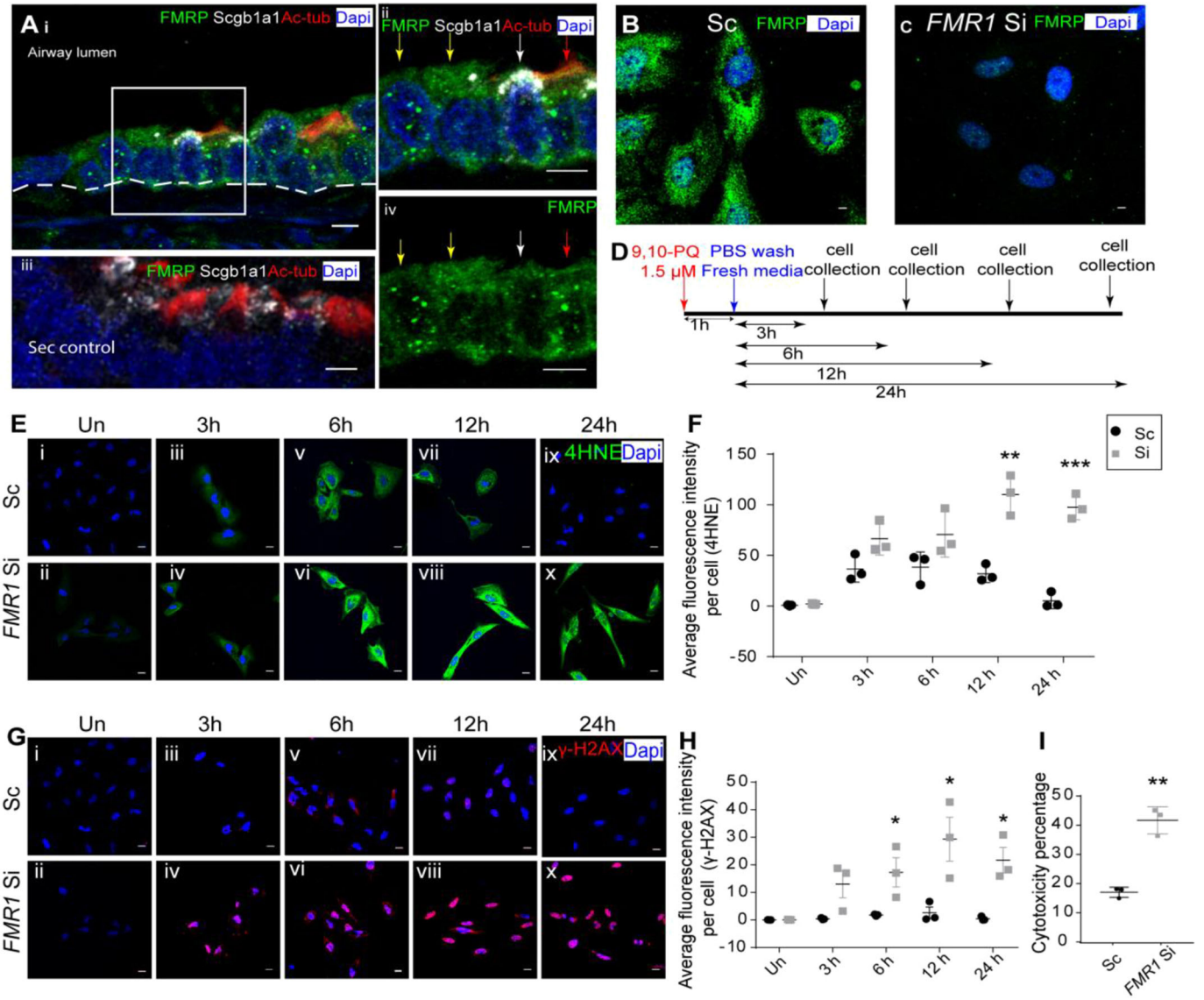

Fig. 4. FMRP is expressed in the human airways and protects human bronchial BEAS-2B cells from PQ-induced stress. (A–C) FMRP expression in the human lung and in BEAS-2B cells, a cell line derived from the human bronchial epithelium. (Ai–iv) FMRP immunostaining (green) in the distal airways of the human lung. (Ai,ii,iv) Stained section showing FMRP expression in airway non-ciliated cells [Scgb1a1$^+$ (white), white arrows; Scgb1a1$^-$, yellow arrows] and ciliated cells (red, red arrow). The white dashed line indicates airway epithelium. The boxed area in i is shown at higher magnification in ii and iv. Negative control [secondary antibody (Sec) alone] for FMRP immunostaining is shown in iii. (B) FMRP immunostaining (green) of BEAS-2B cells (control, scrambled siRNA-treated, Sc). (C) FMRP immunostaining (green) of *FMR1* siRNA-treated BEAS-2B cells. (D–I) Susceptibility of BEAS-2B cells to PQ injury in control (scrambled siRNA-treated, Sc) and *FMR1* siRNA-treated (Si) cells. (D) Schematic showing regimen for PQ injury. (E–H) Expression of markers of oxidative (4HNE) and genotoxic (γ-H2AX) stress in Sc and Si cells prior to and post PQ. Un, uninjured. (Ei–x) 4HNE immunostaining (green) in Sc and Si cells prior to and post PQ. (F) Quantification of 4HNE immunofluorescence per cell in Sc and Si cells prior to and post PQ (*n*=3 experiments). (Gi–x) γ-H2AX immunostaining (red) in Sc and Si cells prior to and post PQ. (H) Quantification of γ-H2AX immunofluorescence per cell in Sc and Si cells prior to and post PQ. (I) Cytotoxicity of PQ in Sc and Si cells 24 h post PQ exposure (*n*=3 experiments). For immunofluorescence analysis, ≥25 cells were analyzed per timepoint per experiment. Graphical data represent mean±s.e.m. Black circles, Sc; gray squares, Si. **P*<0.05; ***P*<0.01; ****P*<0.001 (unpaired two-tailed *t*-test). For normality tests and two-way ANOVA, see Table S4. Scale bars: 5 µm.

A major finding of our study is that FMRP is required for the actuation of the ISR pathway. The mechanism by which FMRP regulates this step is currently unknown. We find that the stress-responsive kinase PKR is activated in FMRP-deficient cells but that the phosphorylation of the PKR substrate, eIF2α, is perturbed. This suggests that the role of FMRP may be downstream to the activation of stress-responsive kinases. The analysis of FMRP-binding proteins in neuronal and other tissues has identified numerous interacting partners. Among these interacting partners are the proteins Caprin1 and G3BP1, which have independently been implicated in the induction of the ISR pathway in response to stress (Taha et al., 2020; Wu et al., 2016). Pertinently, both Caprin1 and G3BP1 have been shown to be important for eIF2α phosphorylation (Reineke et al., 2015; Solomon et al., 2007). Thus, it is plausible that FMRP acts in concert with Caprin1 and G3BP1 to facilitate eIF2α phosphorylation. Although eIF2α phosphorylation is an early event in the ISR pathway and perturbations at this stage are likely to affect all downstream processes, our data do not allow us to rule out the possibility that FMRP has independent roles either upstream

Journal of Cell Science (2022) 135, jcs258652. doi:10.1242/jcs.258652

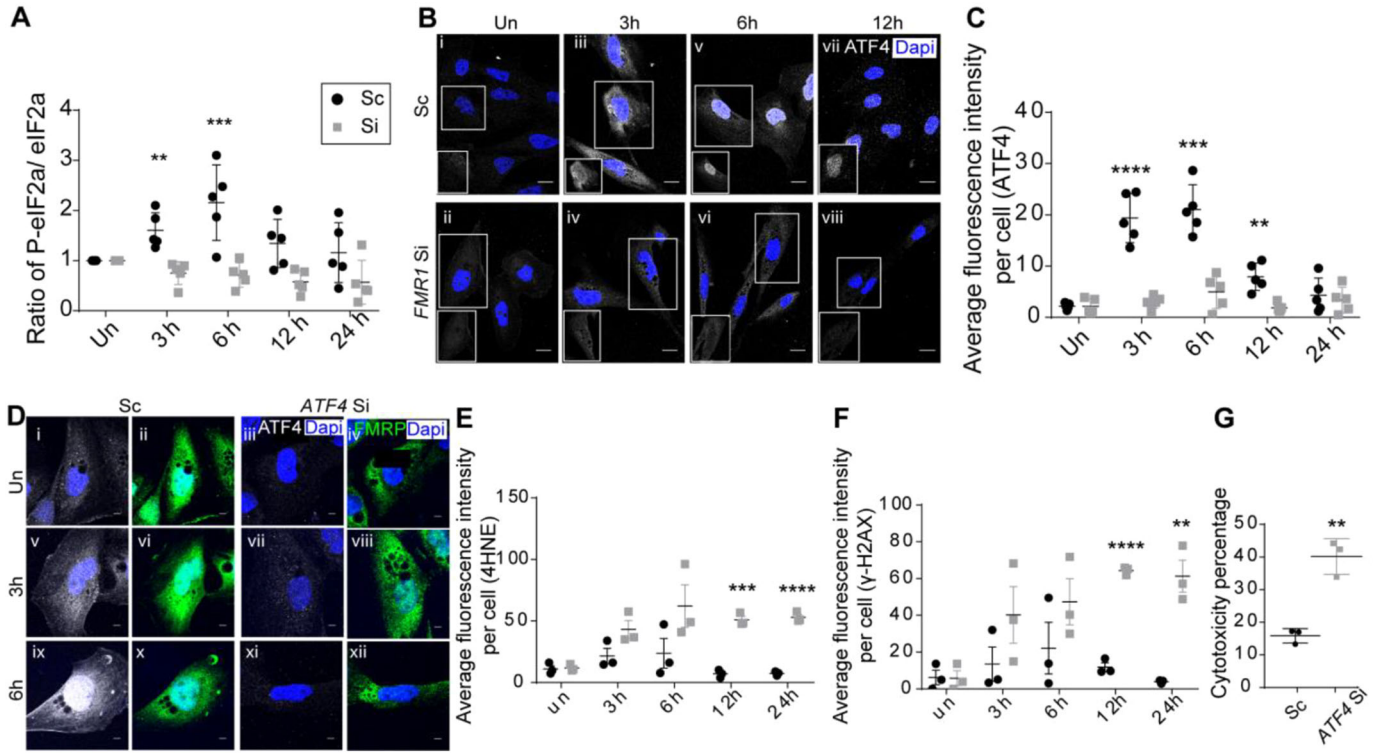

Fig. 5. FMRP-deficient BEAS-2B cells fail to upregulate the integrated stress response and to induce ATF4, essential for protection from PQ-induced stress. (A) Western blot-based quantification of phospho-eIF2α:eIF2α ratios in Sc and Si cells prior to and post PQ treatment (n=5 experiments). Un, uninjured. See Fig. S4A,B for representative blots used for quantification. (B,C) Analysis of ATF4 prior to and post PQ. (Bi–viii) ATF4 immunostaining (white) in Sc (i,iii,v,vii) and Si (ii,iv,vi,viii) cells prior to and post PQ treatment. Note nuclear accumulation of ATF4 in Sc cells by 6 h post PQ treatment (inset). (C) Quantification of ATF4 immunofluorescence per cell in Sc and Si cells prior to and post PQ (n=5 experiments). (D–G) Susceptibility of BEAS-2B cells to PQ in control (scrambled siRNA-treated, Sc) and *ATF4* siRNA-treated (Si) cells. (Di–xii) Analysis of ATF4 levels (white) and FMRP levels (green) in Sc (i,ii,v,vi,ix,x) and Si (iii,iv,vii,viii,xi,xii) cells prior to and post PQ treatment. (E) Quantification of 4HNE immunofluorescence per cell in Sc and Si. See Fig. S4G for representative images. (F) Quantification of γ-H2AX immunofluorescence per cell in Sc and Si. See Fig. S4H for representative images. (G) Cytotoxicity of PQ in Sc and Si cells 24 h post PQ treatment (n=3 experiments). For immunofluorescence analysis, ≥25 cells were analyzed per timepoint per experiment. Graphical data represent mean±s.e.m. Black circles, Sc; gray squares, Si. **P<0.01; ***P<0.001; ****P<0.0001 (unpaired two-tailed t-test). For normality test and two-way ANOVA, see Table S5. Scale bars: 5 µm.

or downstream. Our future experiments will probe these possibilities.

Studies that have examined the role of FMRP vis-à-vis stress responses suggest that FMRP could protect cells from stress in myriad ways. For example, it has been demonstrated that FMRP plays a chromatin-dependent role in inducing the DDR. This could be relevant in the context of the lung. Along the same lines, there is also evidence that FMRP regulates the expression of superoxide dismutase 1 (SOD1) in the brain (Bechara et al., 2009). Levels of SOD1 are reduced in the brains of *Fmr1* KO animals. As SOD1 has an important role in protecting cells from stress, FMRP could alter the susceptibility of tissues to stressful stimuli by altering the baseline levels of SOD1. To investigate this possibility, we probed levels of SOD1 in the brain and lung using both western blot and immunohistochemical approaches (Fig. S6). Although we did observe that SOD1 levels in the brain were lower in *Fmr1* KO than wild type, the levels of SOD1 in the lung were comparable (Fig. S6A,B). Moreover, we also analyzed SOD1 levels in the bronchial cell lines (C22 and BEAS-2B) with or without FMRP to find that SOD1 levels were comparable (Fig. S6D–I). Taken together, these data show FMRP is unlikely to regulate SOD1 expression in the lung. Nevertheless, the role of FMRP in the DDR (Alpatov et al., 2014), and in the regulation of SOD1 expression in the brain, show that FMRP can contribute towards protecting tissues from stress by ISR-independent mechanisms as well.

Although FMRP is expressed in many tissues in humans and mice alike (https://www.genecards.org/cgi-bin/carddisp.pl?gene=FMR1), historically, FMRP has almost exclusively been studied in a neural context because of its connection with intellectual disability. An important finding of this study is that it demonstrates a role for FMRP in the lung. Although the data implicating a role for FMRP in the human lung is based on findings in cell lines and requires validation in more physiologic assays, the data clearly point towards a potential vulnerability in individuals with an *FMR1* deficiency. Clinically, the bulk of the case studies on FXS patients are derived from geographic regions where the load of pulmonary environmental stressors is low. Our study suggests that individuals with FXS living in areas of higher pollutant load may be more susceptible to lung damage and disease, and FMRP status in the lung may be a strong correlate of resilience to pulmonary insults.

MATERIALS AND METHODS

All animal work reported here has been approved by the Internal Animal Users Committee (IAUC) and the Institutional Animal Ethics Committee (IAEC) at inStem. Any procedure that could conceivably cause distress to the animals employed pre-procedural anesthesia with isoflurane gas (Baxter Healthcare Corp.), delivered by an anesthetic vaporizing machine. All animals were monitored for signs of distress and killed if in distress. The analysis of human biopsies was approved by the Institutional Ethics Committee of JSS Medical College.

Journal of Cell Science (2022) 135, jcs258652. doi:10.1242/jcs.258652

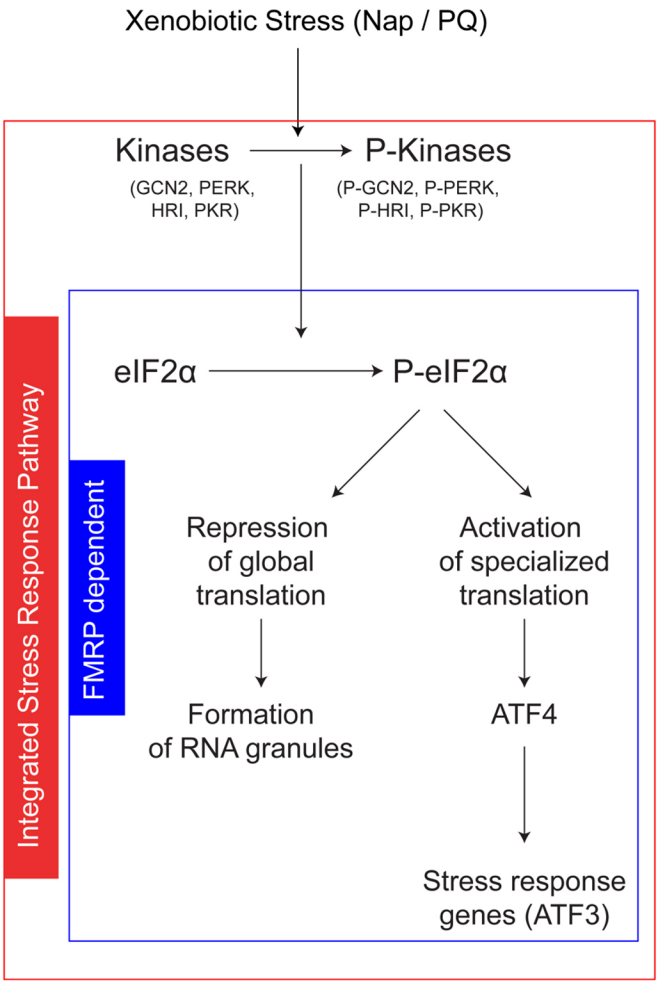

Fig. 6. Model for the role of FMRP in the regulation of the integrated stress response in the lung. Exposure to xenobiotics such as Nap and PQ result in the activation of at least one of four stress-responsive kinases (GCN2, PERK, PKR, HRI) and in the induction of the ISR pathway (outlined in red). Our findings suggest that FMRP has an essential role downstream of phosphorylation of kinases (outlined in blue).

Mouse strains

An *Fmr1* knockout (Fmr1 tm1 Cgr) mouse (*Mus musculus*) strain was maintained on a C57BL/6J background at Brain Development and Disease Mechanisms (BDDM), inStem. Genotyping of the animals was performed using established protocols (Bakker et al., 1994).

Human samples

Human (*Homo sapiens*) lung tissue was obtained from five subjects at autopsy by a forensic pathologist from JSS Medical College, Mysore. The cause of death was not attributed to lung trauma. De-identified samples were fixed in 4% paraformaldehyde (PFA) at 4°C overnight, embedded in paraffin, and processed for immunohistochemical analysis. All human tissues were obtained following due protocols and all clinical investigations have been conducted according to the principles expressed in the Declaration of Helsinki.

Cell lines and culture conditions

Human lung (BEAS-2B) non-ciliated airway epithelial origin cell line and human alveolar basal epithelial adenocarcinomic (A549) cell line were obtained from Johns Hopkins University (kind gifts from Prof. Shyam Biswal, Department of Environmental Health and Engineering, Johns Hopkins Bloomberg School of Public Health, USA; Singh et al., 2009, 2013). The murine club cell line (C22) was purchased from ECACC, UK (cat. no. 07021401, #07D022). All cell lines were tested for mycoplasma contamination and found to be negative. BEAS-2B were grown in DMEM: F12K (Gibco, USA, 21127030) (1:1) medium and A549 cells were grown in DMEM, supplemented with 10% FBS (Gibco, USA, 10082147) and penicillin-streptomycin (Gibco, USA, 1540122) at 37°C and 5% CO_2. The C22 cell line was maintained in a proliferative state as per the supplier's instructions, and experiments were performed 24 h post differentiation. Experiments were conducted within the 3rd to 7th passages for BEAS-2B and A549, and within the 3rd to 12th passages for C22.

Models for xenobiotic stress

For Nap injury in mice, wild-type or *Fmr1* KO mice aged ≥8 weeks of age (2 males and 1 female per timepoint per genotype) were injected intraperitoneally with corn oil (vehicle, Sigma, USA, C8267) or with Nap dissolved in corn oil (300 mg kg^{-1}, Sigma, USA, 147141) using established protocols (Guha et al., 2014, 2012). Animals were killed 12 h, 24 h or 48 h after injection for analysis.

To establish an assay for Nap injury in C22 cells, we first determined that these cells expressed Cyp2f2, which converts Nap to stress-inducing derivatives. Having established this, we tested a range of concentrations of Nap (50 µg ml^{-1} to 500 µg ml^{-1}, in DMSO in DMEM). Nap was found to be stable in solution at concentrations up to 100 µg ml^{-1} and unstable at higher concentrations, leading to cell death within 3 h post exposure. Nap exposure at 50–75 µg ml^{-1} (DMSO in DMEM, DMSO final concentration 0.7%) for short (1 h) and long (24 h) duration led to a progressive increase in expression of stress markers and mild cytotoxicity after a 24 h period. To probe the effects of FMRP or ATF4 deficiency on susceptibility to Nap, cells were exposed to Nap at 75 µg ml^{-1} (DMSO in DMEM, DMSO final concentration 0.7%) for a period of 1 h. Cells were then washed in PBS and chased for varying periods of time in complete medium.

It has been reported previously that PQ causes a sharp decrease in the viability of BEAS-2B cells when administered to cells for 24 h at concentrations greater than 1 µM (Koike et al., 2014). We reconfirmed these findings and determined the LD_{50} to be ∼1.5 µM (Sigma, USA, 275034; dissolved in DMSO in DMEM, DMSO final concentration 0.00002%). To probe the effects of FMRP or ATF4 deficiency on susceptibility to PQ, cells were exposed to PQ at 1.5 µM (DMSO in DMEM, DMSO final concentration 0.00002%) for a period of 1 h. Cells were then washed with PBS, and fresh complete medium was added and chased for varying periods of time in complete medium. A549 cells were also treated with a 1.5 µM dose of PQ for 1 h. Cells were washed with PBS and kept in fresh complete medium and collected at different timepoints for analysis.

siRNA-based knockdown of FMRP, Cyp2f2 and ATF4 expression

Several studies have demonstrated that multiple siRNAs administered together or sequentially work more efficiently for silencing gene expression than a single siRNA (Wang et al., 2016; Fähling et al., 2009; Zhang et al., 2015; Hatch et al., 2010). For our studies we used three or two distinct siRNAs for each targeted gene. siRNAs were administered to cells sequentially, 12 h apart, to silence the gene expression. siRNA transfections were performed with Lipofectamine 2000 (Thermo Fisher Scientific, USA, 11668027). All xenobiotic stress assays in C22 cells were performed 36 h after treatment with the last siRNA. C22 cells were transferred from proliferative to differentiation-inducing medium 12 h after the last siRNA treatment and utilized for xenobiotic stress assays 24 h thereafter. All xenobiotic stress assays in BEAS-2B cells were performed 12 h after treatment with the last siRNA. All siRNAs were obtained from Ambion, USA: murine *Fmr1* (4390771), murine *Atf4* (16708), murine *Cyp2f2* (4390771), human *FMR1* (4392420) and human *ATF4* (16708), and scrambled (negative control, 4390843). The assay IDs for each of the siRNAs are as follows: mouse *Fmr1* siRNA (Assay ID: 5315, 5317, s66177), Human *FMR1* siRNA (Assay ID: 5315, 5316, 5317), mouse *Atf4* siRNA (Assay ID: 160775, 160776, 160777), Mouse *Cyp2f2* siRNA (Assay ID: s64735, s64734), and human *ATF4* siRNA (Assay ID: 122168, 122287, 122372).

Cell cytotoxicity assay

C22 and BEAS-2B cells were inoculated into a 96-well plate and treated with Nap or PQ for 1 h, as described above, and harvested for analysis 24 h later. Cell viability was assayed using WST-1 reagent (Sigma, USA, 5015944001). Briefly, cells were incubated with WST-1 for 4 h and absorbance readings were taken and analyzed as per the manufacturer's protocols. Cytotoxicity percentage=100 [(OD (450 nm–650 nm) of untreated cells – OD (450 nm–650 nm) of treated cells)/OD (450 nm–650 nm) of untreated cells].

Histology, immunofluorescence and imaging

Lungs were inflated with 4% (w/v) PFA (Alfa Aesar, USA, 30525-89-4) in PBS and fixed for 8 h at 4°C. Fixed lungs were subsequently embedded in paraffin, sectioned (5 µm) and processed for immunohistochemical analysis post heat-mediated antigen retrieval at pH 6.0 (Vector Labs, USA, H-3300) except for sections stained with anti-SOD1 antisera, which were subject to antigen retrieval at pH 9.0 (Vector Labs, USA, H-3301). For cellular immunostaining, cells were seeded on coated coverslips (0.1% gelatin, Sigma, USA, G9391), as per the manufacturer's protocol. Post treatment, cells were fixed with 4% PFA for 30 min and blocked with 2% FBS, 0.2% BSA and 0.1% Triton X-100 in 1× PBS for 1 h and stained. Primary antibodies were diluted using the same blocking solution. Immunohistochemical analysis utilized the following antisera: rabbit anti-FMRP (Abcam, UK, 17722, 1:500), rabbit anti-FMRP (Sigma, USA, F4055 1:200), goat anti-Scgb1a1 (Santa Cruz, USA, Sc365992, 1:500), mouse anti-acetylated tubulin (Sigma, USA, T7451, 1:1000), mouse anti-4HNE (Abcam, UK, ab48506, 1:500), rabbit anti-γ-H2AX (Novus Biologicals, USA, NB100-384, 1:1000), mouse anti-Cyp2f2 (Santa Cruz, USA, SC374540, 1:100), mouse anti-ATF4 (Sigma, USA, WH0000468M1, 1:200), rabbit anti-ATF3 (Sigma, USA, HPA001562, 1:200), rabbit anti-SOD1 (Abcam, UK, ab16831, 1:200) and Alexa Fluor 488, 568 or 647-conjugated donkey anti-mouse, -rabbit or -goat IgG secondary antibodies (Invitrogen, USA, A21447, A21202, A21206, A10037, A10042, A31571, 1:300). Stained sections were mounted in ProLong Diamond (Invitrogen, USA, P36962). All samples were imaged on a FV3000 4-laser and FV3000 5-laser confocal microscope or on a Zeiss LSM-780 laser-scanning confocal microscope (Carl Zeiss AG, Germany). For H&E staining, sections were stained with hematoxylin for 10 s and eosin for 30 s, dried and mounted in DPX and imaged on a Nikon Eclipse Ti2 microscope (Nikon, Japan).

Quantitative fluorescence microscopy

Frequencies of club cells/mm of airway, and total cellular fluorescence in club cells, in lung sections, were determined from single tiled optical sections acquired on a confocal microscope using ImageJ software. For club cell frequency analysis, cells attached to the basement membrane were counted per section per animal. Total cellular fluorescence intensity was calculated by subtracting a 'background' value per section from the integrated density per cell (outlined using the software) (for FMRP, 4HNE, γ-H2AX and ATF4). The 'background' value was determined by sampling integrated density of regions on the section devoid of cells. Total cellular fluorescence of C22 and BEAS-2B cells was estimated from single optical sections on a confocal microscope using ImageJ software. In all experiments involving C22, BEAS-2B and A549 cells, ≥25 cells were analyzed per timepoint, per experiment. The images of Scgb1a1 and Cyp2f2 expression in C22 cells are maximum intensity projection images of z-stacks acquired on a confocal microscope.

Western blot analysis

Protein was extracted from cell lysates using RIPA buffer (Thermo Fisher Scientific, USA, 89900) containing Sigmafast EDTA-free protease inhibitor cocktail (Sigma, USA, s8830) and PhosSTOP (Merck, USA, 4906845001). Total protein was run on a 12% SDS PAGE gel, transferred onto a nitrocellulose membrane (Amersham, UK, 10600002), and the membrane was stained with reversible MemCode (Thermo Fisher Scientific, USA, 24580) for total protein estimation [imaged on ImageQuant600 (Amersham, UK) and quantified using ImageJ]. The membrane was subsequently destained, blocked with 5% BSA (Sigma, USA, A9418) for 1 h and probed using the following primary antisera: rabbit anti-Phospho-eIF2α (Ser51) (Cell Signaling Technology, USA, 9721S, 1:1000), mouse anti-eIF2α (Cell Signaling Technology, USA, 2103S, 1:1000), rabbit anti-phospho-PKR (Sigma, USA, SAB4504517, 1:3000), mouse anti-PKR (Santa Cruz, USA, Sc-6282, 1:1000), rabbit anti-GCN2 (Cell Signaling Technology, USA, 3302s), mouse anti-phospho-GCN2 (Cell Signaling Technology, USA, 3301S), rabbit anti-PERK (Cell Signaling Technology, USA, 3192s, 1:1000), rabbit anti-phospho-PERK (Cell Signaling Technology, USA, 3179s), mouse anti-HRI (Santa Cruz, USA, sc-365239). Primary antisera was detected using the following secondary antisera: HRP-conjugated anti-rabbit (Abcam, UK, 6721, 1:3000) and HRP-conjugated anti-mouse secondary (Invitrogen, USA, # 62-6520 1:5000) antibodies and ECL (BioRad, USA, 1620177) and analyzed (imaged on ImageQuant600 and quantified using ImageJ). The levels of eIF2α, phospho-eIF2α, PKR and Phospho-PKR were normalized to the total protein content of the respective lanes. For analysis of SOD1 expression from murine brain and lung tissue lysate, tissues were collected after dissection, washed with PBS and protein was extracted with RIPA buffer and protease inhibitor cocktail. Total protein was run on a 12% SDS PAGE gel and transferred onto a nitrocellulose membrane. We used 5% non-fat dry milk (Santa Cruz, USA, Sc-2325) solution in PBS for blocking and probed the blots with anti-SOD1 (Abcam, UK, ab16831) and anti-β-tubulin (CST, USA, 15115S) antisera. Levels of SOD1 were normalized to corresponding β-tubulin levels.

Quantitative PCR analysis

RNA from cell lysates was extracted using TRIzol (Invitrogen, USA, 15596018, as per the manufacturer's protocol) and qPCR was performed using the primers listed in Table S11. The qPCR assays were constituted with the Maxima SYBR Green/ROX qPCR Master Mix (2×) (Thermo Scientific, USA, K0221) and analyzed on a BioRad CFX3 real-time PCR system (BioRad, USA).

Statistical analysis

Statistical significance of datasets was assessed using unpaired two-tailed *t*-tests post Shapiro–Wilk tests for normality. Data were also analyzed using a two-way ANOVA with a Sidak post-hoc test to compare changes in two groups with respect to time, genotype and interaction parameters. ANOVA data and normality test results for each figure are presented in a tabular format (Tables S1–S10).

Acknowledgements

We thank Joseph Jomon, National Centre for Cell Science (NCCS), Pune for sharing antibodies; Aditya Deshpande, inStem, for assistance in animal experiments; Sarfaraz Nawaz and Sudhriti Ghosh Dastidar, inStem, for their assistance with biochemical analyses; Harlin Kaur, Binita Dam, Arnab Karmakar and Mamta Yadav for technical assistance; and the Central Imaging and Flow Cytometry Facility (CIFF) and Animal Care and Resource Center (ACRC) Facility at Bangalore Life Science Cluster (BLiSC) for their constant support.

Competing interests

The authors declare no competing or financial interests.

Author contributions

Conceptualization: D.S.B., R.B., S. Chavda, R.M., S. Chattarji, R.T., A.B., A.G.; Methodology: D.S.B., R.M., C.V., S. Chattarji, A.G.; Validation: D.S.B., R.B., I.G., S.M.L., R.T., A.B.; Formal analysis: D.S.B., R.M., S. Chattarji, R.T., A.B., A.G.; Investigation: D.S.B., R.B., I.G., S. Chavda, S.M.L., C.V.; Writing - original draft: D.S.B., A.G.; Writing - review & editing: S. Chavda; Visualization: D.S.B., A.G.; Supervision: A.G.; Project administration: D.S.B., A.G.; Funding acquisition: A.G.

Funding

This work was funded by Institute for Stem Cell Science and Regenerative Medicine core funds and the Ramalingaswami Reentry Fellowship (A.G., R.B.), and fellowships from the Department of Biotechnology (S.M.L.), Indian Council of Medical Research (I.G.) and University Grants Commission – Council of Scientific and Industrial Research (D.S.B.).

Peer review history

The peer review history is available online at https://journals.biologists.com/jcs/article-lookup/doi/10.1242/jcs.258652.

References

Alpatov, R., Lesch, B. J., Nakamoto-Kinoshita, M., Blanco, A., Chen, S., Stützer, A., Armache, K. J., Simon, M. D., Xu, C., Ali, M. et al. (2014). A chromatin-dependent role of the fragile X mental retardation protein FMRP in the DNA damage response. *Cell.* **157**, 869-881. doi:10.1016/j.cell.2014.03.040

Bakker, C. E., Verheij, C., Willemsen, R., van der Helm, R., Oerlemans, F., Vermey, M., Bygrave, A., Hoogeveen, A., Oostra, B. A., Reyniers, E. et al. (1994). Fmr1 knockout mice: a model to study fragile X mental retardation. *Cell.* **78**, 23-33. doi:10.1016/0092-8674(94)90569-X

Bechara, E. G., Didiot, M. C., Melko, M., Davidovic, L., Bensaid, M., Martin, P., Castets, M., Pognonec, P., Khandjian, E. W., Moine, H. et al. (2009). A novel function for fragile X mental retardation protein in translational activation. *PLoS. Biol.* **7**, e16. doi:10.1371/journal.pbio.1000016

Buckpitt, A., Boland, B., Isbell, M., Morin, D., Shultz, M., Baldwin, R., Chan, K., Karlsson, A., Lin, C., Taff, A. et al. (2002). Naphthalene-induced respiratory tract toxicity: metabolic mechanisms of toxicity. *Drug. Metab. Rev.* **34**, 791-820. doi:10.1081/DMR-120015694

Demello, D. E., Mahmoud, S., Ryerse, J. and Hoffmann, J. W. (2002). Generation and characterization of a conditionally immortalized lung clara cell line from the H-2Kb-tsA58 transgenic mouse. *In. Vitro. Cell. Dev. Biol. Anim.* **38**, 154-164. doi:10.1290/1071-2690(2002)038<0154:GACOAC>2.0.CO;2

Didiot, M.-C., Subramanian, M., Flatter, E., Mandel, J.-L. and Moine, H. (2009). Cells lacking the fragile X mental retardation protein (FMRP) have normal RISC activity but exhibit altered stress granule assembly. *Mol. Bio. Cell* **20**, 428-437. doi:10.1091/mbc.e08-07-0737

Fähling, M., Mrowka, R., Steege, A., Kirschner, K. M., Benko, E., Förstera, B., Persson, P. B., Thiele, B. J., Meier, J. C. and Scholz, H. (2009). Translational regulation of the human achaete-scute homologue-1 by fragile X mental retardation protein. *J. Bio. Chem.* **284**, 4255-4266. doi:10.1074/jbc.M807354200

Guha, A., Vasconcelos, M., Cai, Y., Yoneda, M., Hinds, A., Qian, J., Li, G., Dickel, L., Johnson, J. E., Kimura, S. et al. (2012). Neuroepithelial body microenvironment is a niche for a distinct subset of Clara-like precursors in the developing airways. *Proc. Natl. Acad. Sci. USA* **109**, 12592-12597. doi:10.1073/pnas.1204710109

Guha, A., Vasconcelos, M., Zhao, R., Gower, A. C., Rajagopal, J. and Cardoso, W. V. (2014). Analysis of Notch signaling-dependent gene expression in developing airways reveals diversity of Clara cells. *PLoS. ONE* **9**, e88848. doi:10.1371/journal.pone.0088848

Guha, A., Deshpande, A., Jain, A., Sebastiani, P. and Cardoso, W. V. (2017). Uroplakin 3a+ cells are a distinctive population of epithelial progenitors that contribute to airway maintenance and post-injury repair. *Cell Rep.* **19**, 246-254. doi:10.1016/j.celrep.2017.03.051

Hatch, E. M., Kulukian, A., Holland, A. J., Cleveland, D. W. and Stearns, T. J. (2010). Cep152 interacts with Plk4 and is required for centriole duplication. *Cell Biol.* **191**, 721-729. doi:10.1083/jcb.201006049

He, C. H., Gong, P., Hu, B., Stewart, D., Choi, M. E., Choi, A. M. K. and Alam, J. (2001). Identification of activating transcription factor 4 (ATF4) as an Nrf2-interacting protein. Implication for heme oxygenase-1 gene regulation. *J. Biol. Chem.* **276**, 20858-20865. doi:10.1074/jbc.M101198200

Koike, E., Yanagisawa, R. and Takano, H. (2014). Toxicological effects of polycyclic aromatic hydrocarbons and their derivatives on respiratory cells. *Atmos. Environ.* **97**, 529-536. doi:10.1016/j.atmosenv.2014.04.003

Konsavage, W. M., Zhang, L., Wu, Y. and Shenberger, J. S. (2012). Hyperoxia-induced activation of the integrated stress response in the newborn rat lung. *Am. J. Physiol. Lung. Cell. Mol. Physiol.* **302**, L27-L35. doi:10.1152/ajplung.00174.2011

Lavrich, K. S., Corteselli, E. M., Wages, P. A., Bromberg, P. A., Simmons, S. O., Gibbs-Flournoy, E. A. and Samet, J. M. (2018). Investigating mitochondrial dysfunction in human lung cells exposed to redox-active PM components. *Toxicol. Appl. Pharmacol.* **342**, 99-107. doi:10.1016/j.taap.2018.01.024

Linder, B., Plöttner, O., Kroiss, M., Hartmann, E., Laggerbauer, B., Meister, G., Keidel, E. and Fischer, U. (2008). Tdrd3 is a novel stress granule-associated protein interacting with the Fragile-X syndrome protein FMRP. *Hum. Mol. Genet.* **17**, 3236-3246. doi:10.1093/hmg/ddn219

Pakos-Zebrucka, K., Koryga, I., Mnich, K., Ljujic, M., Samali, A. and Gorman, A. M. (2016). The integrated stress response. *EMBO Rep.* **17**, 1374-1395. doi:10.15252/embr.201642195

Reineke, L. C., Kedersha, N., Langereis, M. A., van Kuppeveld, F. J. M. and Lloyd, R. E. (2015). Stress granules regulate double-stranded RNA-dependent protein kinase activation through a complex containing G3BP1 and Caprin1. *M. Bio.* **6**, e02486-14. doi:10.1128/mBio.02486-14

Santoro, M. R., Bray, S. M. and Warren, S. T. (2012). Molecular mechanisms of fragile X syndrome: a twenty-year perspective. *Annu. Rev. Pathol.* **7**, 219-245. doi:10.1146/annurev-pathol-011811-132457

Sarcinelli, C., Dragic, H., Piecyk, M., Barbet, V., Duret, C., Barthelaix, A., Ferraro-Peyret, C., Fauvre, J., Renno, T., Chaveroux, C. et al. (2020). ATF4-Dependent NRF2 transcriptional regulation promotes antioxidant protection during endoplasmic reticulum stress. *Cancers* **12**, 569. doi:10.3390/cancers12030569

Singh, A., Ling, G., Suhasini, A. N., Zhang, P., Yamamoto, M., Navas-Acien, A., Cosgrove, G., Tuder, R. M., Kensler, T. W., Watson, W. H. et al. (2009). Nrf2-dependent sulfiredoxin-1 expression protects against cigarette smoke-induced oxidative stress in lungs. *Free. Radic. Biol. Med.* **46**, 376-386. doi:10.1016/j.freeradbiomed.2008.10.026

Singh, A., Happel, C., Manna, S. K., Acquaah-Mensah, G., Carrerero, J., Kumar, S., Nasipuri, P., Krausz, K. W., Wakabayashi, N., Dewi, R. et al. (2013). Transcription factor NRF2 regulates miR-1 and miR-206 to drive tumorigenesis. *J. clin. Investing.* **123**, 2921-2934. doi:10.1172/JCI66353

Solomon, S., Xu, Y., Wang, B., David, M. D., Schubert, P., Kennedy, D. and Schrader, J. W. (2007). Distinct structural features of Caprin-1 mediate its interaction with G3BP-1 and its induction of phosphorylation of eIF2α, entry to cytoplasmic stress granules, and selective interaction with a subset of mRNAs. *J. Mol. Cell. Bio.* **27**, 2324-2342. doi:10.1128/MCB.02300-06

Stripp, B. R., Maxson, K., Mera, R. and Singh, G. (1995). Plasticity of airway cell proliferation and gene expression after acute naphthalene injury. *Am. J. Physiol.* **269**, L791-L799. doi:10.1152/ajplung.1995.269.6.L791

Taha, M. S., Haghighi, F., Stefanski, A., Nakhaei-Rad, S., Kazemein Jasemi, N. S., Al Kabbani, M. A., Görg, B., Fujii, M., Lang, P. A., Häussinger, D. et al. (2020). Novel FMRP interaction networks linked to cellular stress. *FEBS J.* **288**, 837-860. doi:10.1111/FEBS.15443

van 't Wout, E. F. A., Hiemstra, P. S. and Marciniak, S. J. (2014). The integrated stress response in lung disease. *Am. J. Respir. Cell. Mol. Bio.l* **50**, 1005-1009. doi:10.1165/rcmb.2014-0019TR

Van Winkle, L. S., Buckpitt, A. R., Nishio, S. J., Isaac, J. M. and Plopper, C. G. (1995). Cellular response in naphthalene-induced Clara cell injury and bronchiolar epithelial repair in mice. *Am. J. Physiol.* **269**, L800-L818. doi:10.1152/ajplung.1995.269.6.L800

Wang, Z., Sun, W., Cao, J., Cui, H. and Ma, Z. (2016). Repeated Aurora-A siRNA transfection results in effective apoptosis of A549 cells compared to single transfection. *Clin. Lab.* **62**, 697-703. doi:10.7754/clin.lab.2015.150836

Wong, H. R. and Wispe, J. R. (1997). The stress response and the lung. *Am. J. Physiol.* **273**, L1-L9. doi:10.1152/ajplung.1997.273.1.L1

Wu, Y., Zhu, J., Huang, X. and Du, Z. (2016). Crystal structure of a dimerization domain of human Caprin-1: insights into the assembly of an evolutionarily conserved ribonucleoprotein complex consisting of Caprin-1, FMRP and G3BP1. *Acta Crystallogr. Sec. D J. Struct. Bio.* **72**, 718-727. doi:10.1107/S2059798316004903

Zhang, P., Abdelmohsen, K., Liu, Y., Tominaga-Yamanaka, K., Yoon, J.-H., Ioannis, G., Martindale, J. L., Zhang, Y., Becker, K. G., Yang, I. H. et al. (2015). Novel RNA- and FMRP-binding protein TRF2-S regulates axonal mRNA transport and presynaptic plasticity. *Nat. Commun.* **6**, 8888. doi:10.1038/ncomms9888

Zhou, Z., Cao, M., Guo, Y., Zhao, L., Wang, J., Jia, X., Li, J., Wang, C., Gabriel, G., Xue, Q. et al. (2014). Fragile X mental retardation protein stimulates ribonucleoprotein assembly of influenza A virus. *Nat. Commun.* **5**, 3259. doi:10.1038/ncomms4259